Studying Wind Flow-Field Around a Triangular Building by CFD and Wind Tunnel

Do N. Ngo, Y. Q. Nguyen, Anh T. Tran, and Hien T. Le

1 Introduction

Studying wind effects on tall building provides essential information for the purposes of designs of structures or natural ventilation of the building. Interaction between wind and building can be studied by experiments in wind tunnels [3, 8, 9], by numerical simulations [4, 10, 11, 13] or by both of them [7]. Those previous studies reported that the cross-sectional shape of the building is one of the most important factors affecting the pressure distribution on the surfaces of the building and the flow structure around the building.

In this studying, we investigated flowfield around a triangular cross-sectional building with a light well on one side and chamfered roof. Baghaei Daemei et al. [3] studied a triangular shaped building with seven different forms to determine the smallest drag coefficient for the design. However, none of their models has a light well.

The flowfield was investigated by numerical simulation with CFD (Computational Fluid Dynamics) technique and compared with results of experiments in a wind tunnel.

D. N. Ngo (✉)
Faculty of Civil Engineering, Ho Chi Minh City University of Technology, VNU-HCM, Ho Chi Minh City, Vietnam
e-mail: 1870018@hcmut.edu.vn

Y. Q. Nguyen
Van Lang University, Ho Chi Minh City, Vietnam

A. T. Tran · H. T. Le
Faculty of Transportation Engineering, Ho Chi Minh City University of Technology, VNU-HCM, Ho Chi Minh City, Vietnam

J. N. Reddy et al. (eds.), *ICSCEA 2019*, Lecture Notes in Civil Engineering 80,
https://doi.org/10.1007/978-981-15-5144-4_96

2 Numerical and Experiment Methods

2.1 Numerical Method

CFD technique was applied to predict flowfield around the building. The air flow was assumed to be steady, incompressible and isothermal which are governed by the continuity and momentum conservation equations [5]. For modeling turbulence, RANS (Reynolds Averaged Navier-Stockes equations) method was used with the following governing equations:

$$\frac{\partial(\rho\bar{u}_i)}{\partial x_i} = 0 \tag{1}$$

$$\frac{\partial(\rho\bar{u}_i)}{\partial t} + \frac{\partial}{\partial x_j}\left(\rho\bar{u}_i\bar{u}_j + \rho\overline{u_i'u_j'}\right) = -\frac{\partial\bar{p}}{\partial x_i} + \frac{\partial\bar{\tau}_{ij}}{\partial x_j} \tag{2}$$

where $\bar{\square}$ indicates a time-averaged quantity; $\bar{\tau}_{ij}$ are the mean viscous stress tensor components:

$$\bar{\tau}_{ij} = \mu\left(\frac{\partial\bar{u}_i}{\partial x_j} + \frac{\partial\bar{u}_j}{\partial x_i}\right) \tag{3}$$

The eddy-viscosity model was used for the Reynolds stress $\rho\overline{u_i'u_j'}$ with two equations for the turbulent kinetic energy k and the dissipation ε [5]. Equations (2) and (3) were discretized on an unstructured mesh using Finite Volume Method with the ANSYS Fluent code. Three RANS models: Standard k–ε, k–ε RNG, k–ω SST were used to simulate and the results were compared with experiments in this study.

The studied building had a triangular cross section and a chamfered roof. The prototype building was 366-m high and 77-m wide for each of its triangular length. There was a light well on one side of the building. The studied building is scaled to assure the similar conditions as experiments in the wind tunnel. A scaled model of the building was made at a scaling ratio of 1:750 resulting in a studied model of 0.488 m height and 0.1027 m width, as shown in Fig. 1a The light well is on onside of the building and between the surfaces M3 and M4.

Inside the computational domain, only the building was considered. Surrounding structures were not modeled. As suggested by [6, 12] for computations for single building, the computational domain was extended to 5H to the top and lateral boundaries except for the outflow boundary behind the building where it was set to 15H. Figure 1b shows the size of computational domain.

To reproduce the experiments in the wind tunnel, uniform velocity profile was set at the inlet with a turbulence intensity of 5%. At the lateral and top sides, free stress conditions were used. Zero normal gradients of the flow were assumed at the outflow boundary.

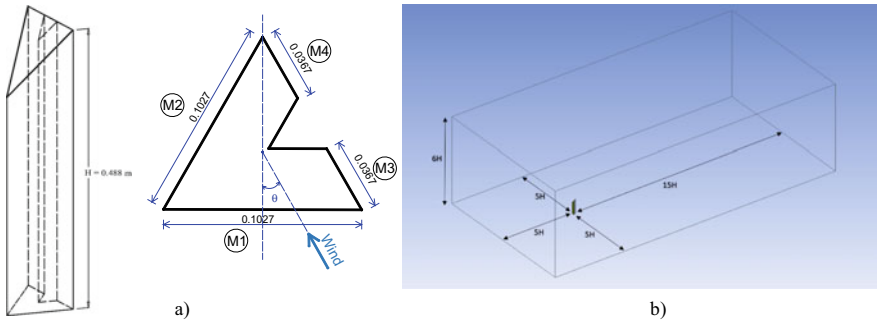

Fig. 1 The studied building: **a)** scaled 3D model of the building and its cross-sectional area with dimensions in meter, **b)** the computational size (H is the building height)

Different mesh resolutions were tested and compared the drag on the building. It was found that a mesh with 10^6 elements or more was sufficient for obtaining a grid-independent drag coefficient.

The drag coefficient is defined as:

$$C_d = \frac{F_d}{\frac{1}{2}\rho V_\infty^2 . A_{ref}} \tag{4}$$

where F_d is the force acting parallel to the wind direction; ρ is the fluid density; V_∞ is the steady wind speed in front of the building, A_{ref} is the reference area which is the frontal area of the building.

2.2 *Experiment Method*

The experiments were conducted in an open wind tunnel at the Laboratory of Building Physics and Fluid Mechanics of the Ho Chi Minh City University of Technology. The test section of the wind tunnel had an area of 1.0 m × 1.0 m and a length of 2.0 m. The working wind speed was 6.0 m/s. With the above scaling ratio and the characteristics of the wind tunnel, the Reynolds number based on the height H of the model was 1.83×10^4 and the blockage ratio was 4.98%. These conditions satisfied the recommendations by [1].

The model was placed on the turn table in the test section of the wind tunnel. Different wind angle θ relative to the surface M1 of the model, as indicated in Fig. 1.a, was tested. At each wind angle, pressure on four surfaces of the model, from M1 to M4, was recorded at 27 points on the M1 and M2 faces and 10 points on the M3 and M4 faces together with the static pressure of the wind flow. The wind speed and static pressure was measured at a distance of 0.5 m in front of the model. Figure 2b shows distribution of pressures taps on each face of the model.

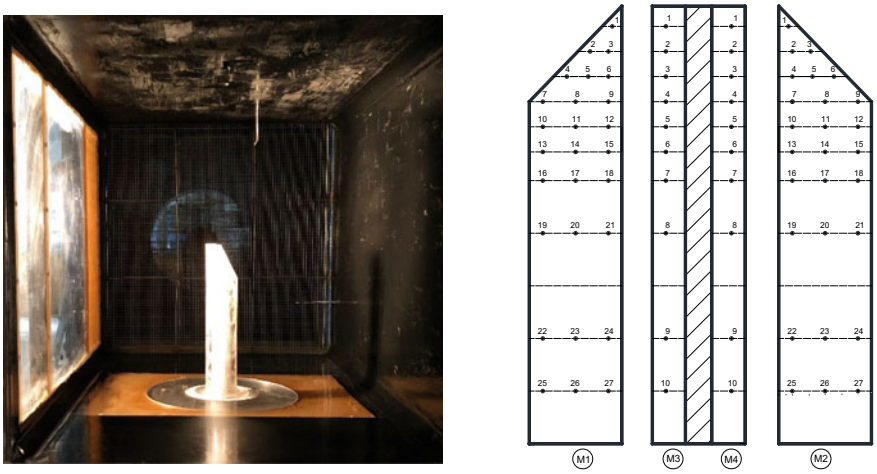

a) b)

Fig. 2 **a)** Scaled model in the wind tunnel, **b)** distribution of pressure taps on each face

The pressures were recorded by sensors having a resolution of 0.3 Pa and an accuracy of 1%. The sensors were connected to a data logger which had a sampling rate of 1 Hz and recorded signals continuously. The recorded data was analyzed to obtained time-averaged pressure and wind speed. The averaged interval was 5-minute which was found to be sufficient to achieve time-independent statistics.

From the measured data, pressure coefficient C_p at each point on the surfaces of model was obtained:

$$C_p = \frac{p - p_\infty}{\frac{1}{2}\rho V_\infty^2} \tag{5}$$

where p is the measured pressure on the model surface; and p_∞ is the static pressure of the wind flow.

2.3 Results and Discussions

Pressure distribution on the surfaces of the studied building.

For validating the computational model, mean pressure coefficients C_p at 2/3 height of the building at two wind angles: $\theta = 0°$ and $\theta = 120°$ were compared with the experimental data. Figure 3 shows mean pressure coefficients C_p at 2/3 H of the building. The studied building had an equilateral triangular cross-section. Dx is the length of a side. (Dx = 0.1027 m).

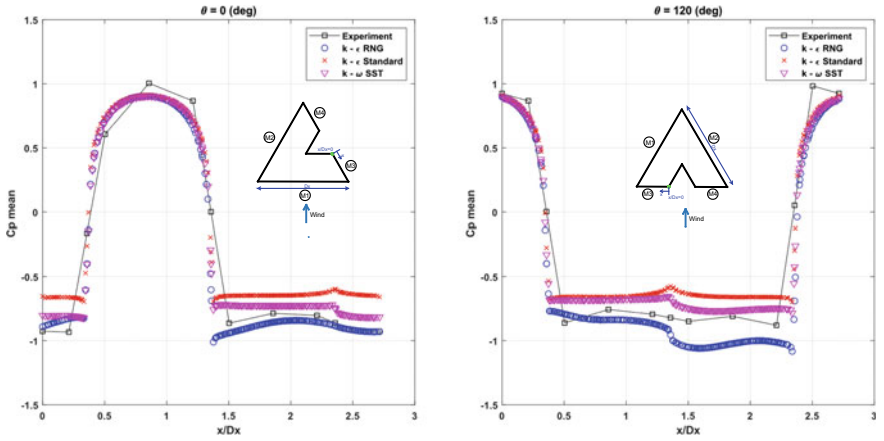

Fig. 3 Mean pressure coefficients C_p at 2/3 H of the building

On the front surface of the building at both of wind angles, the present computational results of three RANS models (standard k–ε, k–ε RNG, k–ω SST) and the experimental data are in good agreement with minor discrepancy. It is noted that the pressure coefficient distributions from all three RANS models are identical.

There are substantial discrepancies between computational and experimental results on the back and side surfaces. On the back and the side surfaces in the case with the wind angle: $\theta = 0°$, the pressure coefficient distributions predicted by the k–ε RNG model and the k–ω SST model are close to those of the measurements. Whereas, the results from the standard k–ε model and the measurements do not agree well.

In the case with the wind angle: $\theta = 120°$, the pressure coefficient distributions predicted with three RANS models are seen in fairly good agreement with the data of the experiments on the M1 side face. However, there are substantial differences in prediction on the M2 side face among the RANS models. The k–ω SST model is the closest to the measurements. Discrepancies between computed and experimental data on the leeward sides of the building may be due to the errors in the wind speed measurement and other routine errors. Moreover, the flow structure behind the model is unsteady, which is hard to predict all accurately by steady RANS methods as employed in this study.

Figures 4, 5 and 6 show the distributions of measured pressure coefficient on the surfaces of the model at different wind angle. On each surface, the pressure coefficient C_p varies strongly with the wind angle. It is observed that C_p is positive on the windward surfaces and negative on the leeward sides, as can be expected.

Effects of the light well on pressure distribution can be seen for the case of $\theta = 0°$. The pressure coefficient on the M2 surface was less negative on the M3-M4 surfaces. When the wind flow was normal to a surface ($\theta = 0°$ for M1, $\theta = 240°$ for M2, and $\theta = 120°$ for M3-M4), the pressure coefficient on M1 and M2 have similar values while that on the M3-M4 is sufficiently lower. Therefore, it is expected that

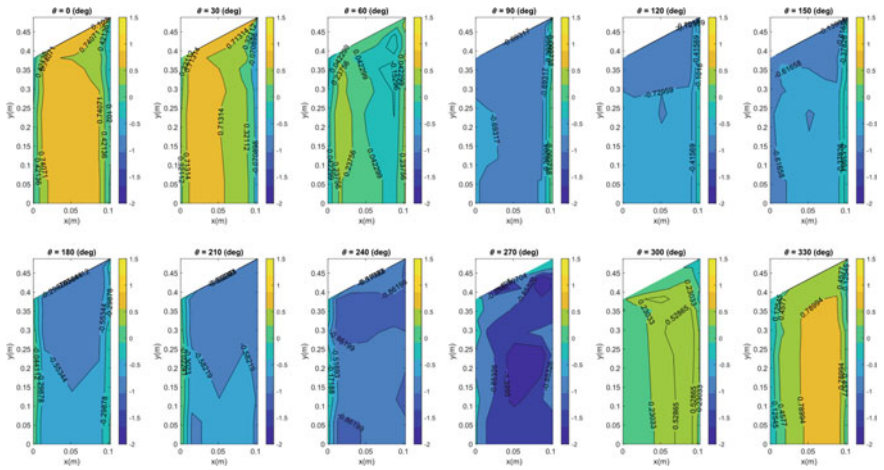

Fig. 4 Distributions of C_p on the M1 surface (experiment)

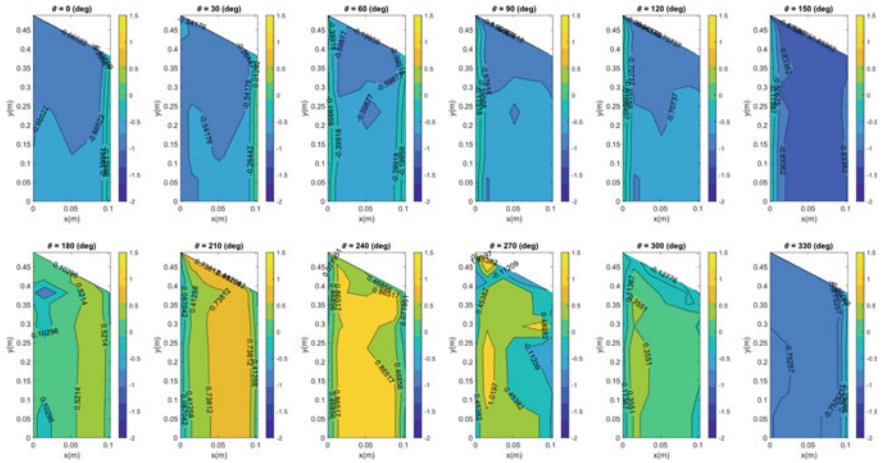

Fig. 5 Distributions of C_p on the M2 surface (experiment)

the presence of the light well and the chamfered roof reduces the pressure on the M3-M4 surfaces where the light well is located.

The distribution of C_p on M1 for $\theta = 0°$ is similar to that on M2 for $\theta = 240°$. This fact shows good repeatability of the measured data, as from the geometry of the building, these two surfaces should have similar aerodynamic behaviors at such wind angles.

One of the intended functions of the light well is for ventilating the building naturally. As the light well was on one side of the building, single-sided natural ventilation mode [2] is expected. The pressure distribution on M3 and M4 should

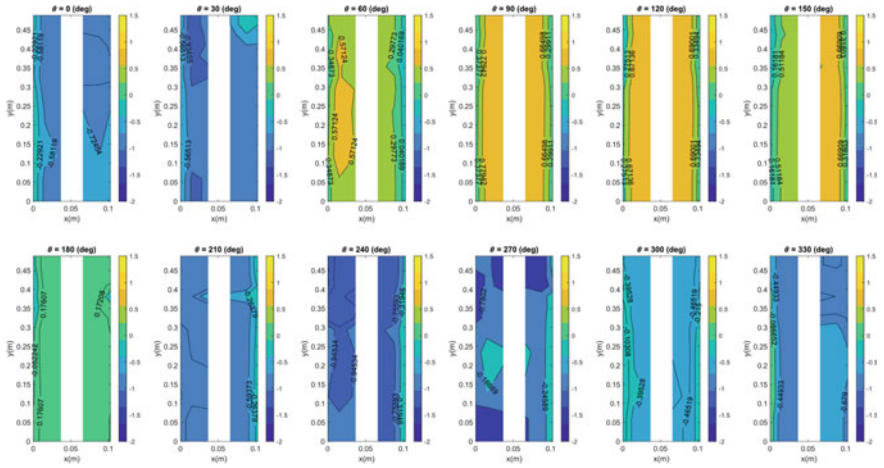

Fig. 6 Distributions of C_p on the M3 and M4 surfaces (experiment)

then have different values so that airflow enters the building on the side with higher pressure and leaves at the other side with lower pressure. From Fig. 6, it is observed that the best wind angle for that purpose is $\theta = 150°$ with maximum difference of C_p between M3 and M4 of about 0.16.

The drag coefficient with different wind angles.

Figure 7 shows the change of drag coefficient C_d with wind angles, which is predicted by k–ε RNG model, k–ω SST model and standard k–ε. The computational results of these models are similar to each other, except for small discrepancies with wind angles: $\theta = 0°$, $\theta = 120°$ and $\theta = 240°$. The drag coefficient of the studied building is maximum with wind angle $\theta = 120°$ and minimum with wind angles: $\theta = 60°$, $\theta = 180°$ and $\theta = 300°$. The drag coefficient C_d varies strongly with angle; hence is strongly dependent on the shape of the windward surface.

Flow structure around the building

Figure 8a, b presents the flow structure behind the model visualized by smoke in the wind tunnel and by the CFD model. Vortex shedding can be seen with the smoke as well as the computed flowfield. This phenomenon is also well studied and reported before [4, 8].

Figure 9 shows the streamlines passing the central vertical plane of the model at two wind angles: $\theta = 0°$ and $\theta = 120°$. Different pattern of the wake behind the model can be seen. The difference may be due to two factors: the light well and the chamfered roof.

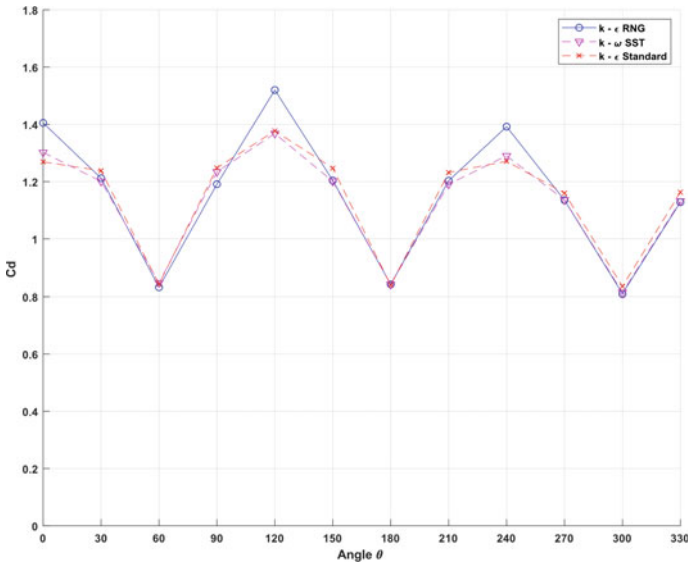

Fig. 7 Drag coefficients C_d with the different wind angles

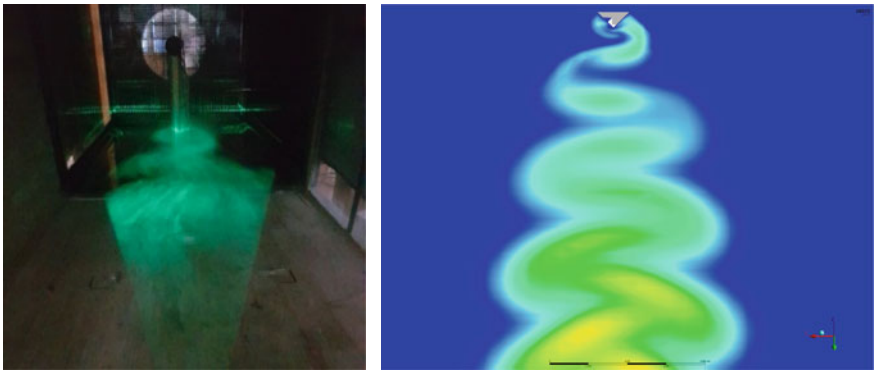

a) b)

Fig. 8 **a)** Smoke visualization, **b)** computed flowfield around the building for the case of $\theta = 0°$

3 Conclusions

By experiments in wind tunnel and by CFD, the flowfield around a triangular cross-sectional building was studied. The results show that the presence of the light well and the chamfered roof reduces the pressure coefficient on the surface of the building and changes the structure of the wake behind the building. The wind angle at which the pressure distribution for the best natural ventilation design of the building with

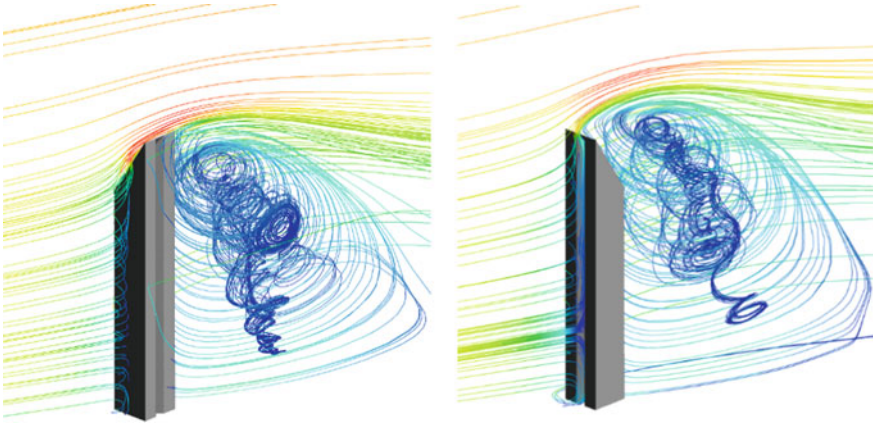

Fig. 9 Computed streamlines in the central vertical plane in the cases of $\theta = 0°$ (left) and $\theta = 120°$ (right)

the light well was found to be $\theta = 150°$. The numerical results show that the k–ω SST model in three studied RANS models exhibits the best at the prediction of mean pressure coefficients. The drag coefficient of the studied building is maximum with wind angle $\theta = 120°$ and minimum with wind angles: $\theta = 60°$, $\theta = 180°$ and $\theta = 300°$.

Acknowledgements The experiments in this research are supported by the Laboratory of Building Physics and Fluid Mechanics of the Ho Chi Minh City University of Technology, VNU-HCM. P. K. Oanh and N. H. T. Loc (PFIEV 2014) are greatly appreciated for their helping the experiments.

References

1. American Society of Civil Engineers (2012). ASCE/SEI 49-12: wind tunnel testing for buildings and other structures
2. Awbi (2003) Ventilation of buildings. Spon Press
3. Baghaei Daemei A, Khotbehsara EM, Nobarani EM, Bahrami P (2019) Study on wind aerodynamic and flow characteristics of triangular-shaped tall buildings and CFD simulation in order to assess drag coefficient. Ain Shams Eng J
4. Elshaer A, Aboshosha H, Bitsuamlak G, El Damatty A, Dagnew A (2016) LES evaluation of wind-induced responses for an isolated and a surrounded tall building. Eng Struct 115:179–195
5. Ferziger JH, Peric M (2002) Computational methods for fluid dynamics. Springer
6. Franke J (2007) Introduction to the prediction of wind loads on buildings by computational wind engineering (CWE). In: Stathopoulos T, Baniotopoulos CC (eds) Wind effects on buildings and design of wind-sensitive structures, vol 493. CISM International Centre for Mechanical Sciences, Springer, pp 67–103
7. Hubova O, Macak M, Konecna L, Ciglan G (2017) External pressure coefficients on the atypical high-rise building—computing simulation and measurements in wind tunnel. Procedia Eng 190:488–495

8. Kim B, Tse KT, Yoshida A, Tamura Y, Chen Z, Van Phuc P, Park HS (2019) Statistical analysis of wind-induced pressure fields and PIV measurements on two buildings. J Wind Eng Ind Aerodyn 188(November 2018):161–174
9. Li Y, Li QS, Chen F (2017) Wind tunnel study of wind-induced torques on L-shaped tall buildings. J Wind Eng Ind Aerodyn 167(September 2016):41–50
10. Tamura T, Nozawa K, Kondo K (2008) AIJ guide for numerical prediction of wind loads on buildings. J Wind Eng Ind Aerodyn 96(10–11):1974–1984
11. Thordal MS, Bennetsen JC, Koss HHH (2019) Review for practical application of CFD for the determination of wind load on high-rise buildings. J Wind Eng Ind Aerodyn 186(October 2018):155–168
12. Tominaga Y, Mochida A, Yoshie R, Kataoka H, Nozu T, Yoshikawa M, Shirasawa T (2008) AIJ guidelines for practical applications of CFD to pedestrian wind environment around buildings. J Wind Eng Ind Aerodyn 96(10–11):1749–1761
13. van Hooff T, Blocken B, Tominaga Y (2017) On the accuracy of CFD simulations of cross-ventilation flows for a generic isolated building: comparison of RANS, LES and experiments. Build Environ 114:148–165